

**PCCP**

Kamlet-Taft solvent parameters, NMR spectroscopic analysis and thermoelectrochemistry of lithium-glyme solvate ionic liquids and their dilute solutions

Journal:	<i>Physical Chemistry Chemical Physics</i>
Manuscript ID	CP-ART-04-2018-002527.R1
Article Type:	Paper
Date Submitted by the Author:	25-May-2018
Complete List of Authors:	Black, Jeffrey; The University of New South Wales, School of Chemistry Dolan, Andrew; University of New South Wales, School of Chemistry Harper, Jason; University of New South Wales, School of Chemistry Aldous, Leigh; King's College London, Department of Chemistry; University of New South Wales, School of Chemistry

SCHOLARONE™
Manuscripts



Journal Name

ARTICLE

Kamlet-Taft solvent parameters, NMR spectroscopic analysis and thermoelectrochemistry of lithium-glyme solvate ionic liquids and their dilute solutions

Received 00th January 20xx,
Accepted 00th January 20xx

DOI: 10.1039/x0xx00000x

www.rsc.org/

Jeffrey J. Black,^a Andrew Dolan,^a Jason B. Harper^a and Leigh Aldous^{*,a,b}

Solvate ionic liquids are a relatively new class of liquids produced by combining a coordinating solvent with a salt. They have a variety of uses and their suitability for such depends upon the ratio of salt to coordinating solvent. This work investigates the Kamlet-Taft solvent parameters of, NMR chemical shifts of nuclei in, and thermoelectrochemistry of a selected set of solvate ionic liquids produced from glymes (methyl terminated oligomers of ethylene glycol) and lithium bis(trifluoromethylsulfonyl)imide at two different compositions. The aim is to improve the understanding of the interactions occurring in these ionic liquids to help select suitable solvate ionic liquids for future applications.

Introduction

Solvate ionic liquids are a relatively new class of ionic liquids composed of at least one complex ion, typically formed by the solvation of a metal salt (usually lithium) with a coordinating solvent (such as glymes), as shown in Figure 1.¹ The ability to form these solvate ionic liquids (as opposed to a concentrated salt solution) is dependent upon the solvent used as a ligand, as well as the counter-ion.¹⁻³

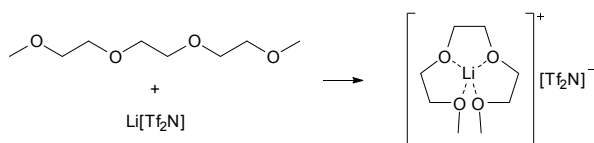


Figure 1. Formation of a solvate ionic liquid from an equimolar amount of a salt and a solvent.

This new class of ionic liquid is primarily being investigated for use as an electrolyte in lithium ion batteries,⁴⁻⁶ and shares numerous desirable properties with conventional ionic liquids including a relatively low volatility, good electrochemical stability and high ionic conductivity,⁷ with their low volatility

being especially important for use in lithium-air batteries.⁸ However, their use is not limited to lithium-based batteries, with these solvents being investigated for other uses such as electrolytes for thermoelectrochemical cells⁹ and as solvents for organic reactions.¹⁰ The solvation dynamics of these systems have been extensively measured, and have indicated that the simple representation in Figure 1 does not accurately portray the typical ligand-ion coordination and dynamics observed in these systems.^{1, 3, 7, 11, 12}

Importantly, the ratio of salt to solvent can have a significant effect on the properties of the mixture, such as the electrochemical and thermal stability,⁸ and the viscosity and conductivity;⁹ this has significant implications upon performance in certain applications, such as (thermo)electrochemical systems.⁹ Certain applications favour the 1:1 'solvate ionic liquid' ratio⁸ whereas others perform better as concentrated electrolyte solutions.⁹ However, there is currently no way of predicting what the optimal ratio of salt to solvent will be for a given application, hence the need for further investigation and the development of predictive tools.

One such tool is the set of Kamlet-Taft solvation parameters (α , β and π^*). These three parameters can be utilised to describe the nature of a solvent system, and are frequently measured using spectrophotometric probe molecules.¹³⁻¹⁵ Linear combinations of the Kamlet-Taft parameters are also being used in the interpretation and prediction of a range of processes, such as dissociation constants of acids in various solvents,^{16, 17} Gutmann's solvent donor and acceptor numbers¹⁸ and, perhaps most relevant to the work described here, electrochemical properties such as redox potentials in different solvents.¹⁹

As such, the study of the Kamlet-Taft solvent parameters of these new solvate ionic liquids is desirable to be able to further these predictions, and to potentially form new relationships between these properties and the various

^a School of Chemistry, UNSW Australia, Sydney, NSW 2052, Australia

^b Department of Chemistry, King's College London, London, SE1 1DB, UK
E-mail: leigh.aldous@kcl.ac.uk

†

Electronic Supplementary Information (ESI) available: Included as supplementary information is a table with several representations of the composition of the solutions tested, details on the derivation of Kamlet-Taft parameters including example spectra, representative NMR spectra of the solutions examined, a table of NMR chemical shifts observed for all species examined, an example measurement for determining the Seebeck coefficient of a lithium-glyme solution, Seebeck coefficients for additional compositions lithium-glyme solutions, details on the derivation of the number of coordinated oxygen atoms and correlations between Kamlet-Taft parameters and the Seebeck coefficients of lithium-glyme solutions., See DOI: 10.1039/x0xx00000x

physicochemical properties and applications of these systems. While there has been considerable study of the Kamlet-Taft parameters of ionic liquids in general,¹⁹⁻²² including some study on mixtures of ionic liquids and organic solvents,²⁰ there has been limited study of the Kamlet-Taft parameters of solvate ionic liquids.^{23, 24}

One technique that has been used extensively to investigate these solvate ionic liquids is NMR spectroscopy. A large portion of these analyses have focused on the diffusion of the species to determine if the system forms either a "good" solvate ionic liquid, where the lithium is solvated in a long lived complex, or a "poor" solvate ionic liquid, where the complex is either transient or does not exist at all.^{1, 3, 7, 11, 12} Other studies have either utilised changes in chemical shifts of the nuclei in the anions and cations of similar systems to determine ion pairing constants,^{25, 26} or used the change in chemical shift of the glyme to determine the proportion of free glyme²⁷ without significant discussion of the origin of the change in chemical shift. The study of the chemical shift of nuclei in these systems should give insight into interactions between the lithium ion and glyme ligand with different glymes and at different concentrations.

An additional parameter that can provide insight into the interactions occurring between the lithium ion and the glyme molecules is the temperature dependence of the redox potential, which is fundamentally related to the solvation dynamics occurring in the solution.^{28, 29} This relationship is primarily based upon the entropy change during the redox process (ΔS), which is typically dominated by solvent rearrangement, and can be quantified as the temperature coefficient of the electrode potential (the change in electrode potential (ΔV) resulting from a change in temperature (ΔT)), or Seebeck coefficient (S_e), as shown in Equation 1; n is the number of electrons involved in the redox process and F is Faraday's constant.^{28, 29}

$$S_e = \Delta V / \Delta T = \Delta S / nF \quad (1)$$

This temperature dependent behaviour also has significant implications for the operation of electrochemical devices such as lithium ion batteries.^{30, 31} Importantly, this behaviour could also be directly applied to the thermoelectrochemical conversion of waste thermal energy into electrical energy.⁹

This manuscript examines in parallel each of these different ways to characterise these new systems.

Experimental

Lithium bis(trifluoromethylsulfonyl)imide ($\text{Li}[\text{Tf}_2\text{N}]$) was obtained from IoLiTec (Germany). 1,2-Dimethoxyethane (monoglyme, G1), diethyleneglycol dimethylether (diglyme, G2), and triethyleneglycol dimethylether (G3) were obtained from Sigma Aldrich (Australia). Tetraethyleneglycol dimethylether (G4) was obtained from Tokyo Chemical Institute (Japan). THF was obtained from Chem Supply (Australia) and hexane was obtained from Scharlau (Spain). Lithium discs and CR2032 battery casings were obtained from

MTI Corporation (USA). All chemicals were immediately taken into an argon-filled glovebox upon receipt, with the exception of hexane which was first freeze-pump-thaw degassed, and THF which was dried over sodium and benzophenone and distilled under nitrogen and then freeze-pump-thaw degassed. Once inside the glovebox activated 3 Å molecular sieves were added to ensure the solvents remained dry. Lithium discs were cleaned by scrubbing gently with a toothbrush in hexane for approximately 10 seconds on each face of the disc, following a previously reported cleaning methodology,³² and used immediately thereafter.

The $\text{Li}[\text{Tf}_2\text{N}]$ and glyme solutions were prepared by accurately weighing the components (salt and solvent) in an argon filled glovebox and mixing until fully dissolved. These mixtures will be referred to based upon the solvent (T for THF, G1 to G4 for monoglyme through tetraglyme), as well as a number based upon the ratio of lithium ions per oxygen atoms from the glyme or THF, *e.g.* G3 0.25 indicates a solution of $\text{Li}[\text{Tf}_2\text{N}]$ and triglyme such that there are 0.25 lithium ions for every oxygen atom from the glyme, or 1 mol lithium ions per 1 mol of triglyme. Table S1 displays these ratios, as well as other numerical representations of the composition of these systems.

Kamlet-Taft solvent parameters were measured spectroscopically using three solvchromatic dyes, *N,N*-diethyl-4-nitroaniline, 4-nitroaniline and Richardt's dye (2,6-Diphenyl-4-(2,4,6-triphenyl-1-pyridinio)phenolate). The absorption maxima were determined and the parameters calculated using fitting equations previously reported.^{13-15,j} The errors reported are those based upon an error of 1 nm in the measured wavelength.

¹³C, ¹H and ⁷Li NMR data were obtained on a Bruker Avance III 400 MHz NMR spectrometer at 25 °C, using a capillary filled with lithium acetate in *d*₆-DMSO as a reference. ¹⁷O NMR data was obtained on a Bruker Avance III 600 MHz NMR spectrometer at 60 °C, using a capillary filled with *d*₆-DMSO as a reference. The ¹⁷O NMR spectra were acquired with a spectral width of 400 ppm, pulse duration of 22.5 μs, acquisition time of 15.7 ms and a recycle delay of 20 ms. For the pure solvents, 32 768 scans were acquired. For the dilute solutions and the concentrated solutions of THF and G1, 65 536 scans were acquired. For the remaining solutions 131 072 scans were acquired. The spectra were processed with exponential multiplication with a line broadening of 10 Hz for the pure solvents and 50 Hz for the solutions.

Cells for thermoelectrochemical measurements were prepared as previously reported,⁹ and then tested using an in-house tester, which has also been previously reported.^{33, 34} The cold side of the cell was kept at 20 °C, and the temperature of the hot side was varied as required. During all measurements, the cell was kept on its side, *i.e.* with the thermal gradient horizontal. All measurements were made

ⁱ The α and β parameters were calculated using the wavelength of a single dye with the calculated π^* parameter.

using a Keysight B2901A Precision Source/Measure Unit (TRIO Test & Measurement Pty Ltd, Australia).

The Seebeck coefficient was determined through measuring the open circuit potential for the cell for 1,000 seconds, then averaging the potential over the final 500 seconds, at temperature differences of 10, 20, 30, 40 and 50 K. The initial 500 seconds were to allow the cell to reach the target temperature and stabilise. Seebeck coefficients reported are the averages of multiple measurements with the error being the standard deviation of the measurements.

Results & Discussion

The coordinating solvents chosen for this study were a series of glymes, with increasing chain length; THF was chosen as a substitute for dimethyl ether, which is a gas under standard conditions. The lithium ratios were chosen to provide a range of useful compositions in the final mixture, with the highly concentrated “solvate ionic liquid” cases (0.25 lithium ions per oxygen atom) suited to low current applications³⁵ while providing ionic liquid-like physicochemical properties. These were compared with relatively more dilute solutions (0.025 lithium ions per oxygen atom; molality *ca.* 0.5 mol Li⁺ per kg)ⁱⁱ more suited to higher current applications, such as harvesting waste thermal energy.⁹

Kamlet-Taft solvent parameters

The solvent properties of the ionic liquids were analysed by measuring the UV-Vis absorption maxima of three solvchromatic dyes (individually dissolved in the pure solvents and lithium solutions), and then calculating the Kamlet-Taft solvent parameters (see ESI for full details and figure S1 for an example series of spectra). These parameters for the various solutions considered are shown in Table 1. The values for these parameters are comparable (given the inherent variation between instrumentation and dyes used) to the values previously reported in the literature for the pure solvents^{14, 15, 18, 23, 24} and the G3 based solvate ionic liquid.^{23, 24} Notably, while there has been reported values for a G4 based solvate ionic liquid,^{23, 24} that report used a slightly different ratio to that used in this study; there were no prior reported values for the other lithium-glyme mixtures analysed in this study.

The α parameters of the pure solvents – measures of the hydrogen bond donating ability of the solvent – were *ca.* 0, as would be expected given that the only hydrogens present are upon alkyl chains. Upon formation of the dilute lithium solution (0.025 lithium ions per glyme oxygen atom), the α parameter increased significantly to *ca.* 0.65. This increase is indicative of either the solvated lithium cation interacting with the probe molecule in a manner similar to a hydrogen bond

Table 1. Kamlet-Taft solvent parameters of solvents and solutions analysed. Uncertainties are reported as error due to 1 nm change in measured wavelength.

Substance	α	β	π^*
THF	0.00 ± 0.01	0.56 ± 0.04	0.60 ± 0.02
G1	0.03 ± 0.01	0.66 ± 0.04	0.58 ± 0.02
G2	0.00 ± 0.01	0.68 ± 0.04	0.64 ± 0.02
G3	0.04 ± 0.01	0.66 ± 0.04	0.66 ± 0.02
G4	0.02 ± 0.01	0.66 ± 0.04	0.66 ± 0.02
T 0.025	0.67 ± 0.01	0.60 ± 0.04	0.65 ± 0.02
G1 0.025	0.67 ± 0.01	0.63 ± 0.04	0.68 ± 0.02
G2 0.025	0.64 ± 0.01	0.60 ± 0.04	0.75 ± 0.02
G3 0.025	0.60 ± 0.01	0.62 ± 0.04	0.78 ± 0.02
G4 0.025	0.64 ± 0.01	0.66 ± 0.04	0.75 ± 0.02
T 0.25	0.62 ± 0.01	0.48 ± 0.04	0.81 ± 0.02
G1 0.25	1.17 ± 0.01	0.35 ± 0.03	0.94 ± 0.02
G2 0.25	1.19 ± 0.01	0.29 ± 0.03	0.97 ± 0.02
G3 0.25	1.08 ± 0.01	0.26 ± 0.03	1.00 ± 0.02
G4 0.25	1.22 ± 0.01	0.27 ± 0.03	0.99 ± 0.02

donor, a lithium-solvent complex possessing hydrogen bond donor ability greater than that of the free solvent, or a combination of these two factors. There is no systematic trend in the values for the five dilute systems, although generally α was lower for the longer chain length glymes.

On increasing the lithium content by an order of magnitude to form the ‘solvate ionic liquid’ systems (four oxygen atoms per lithium), the α parameter for the glyme systems nearly doubled, to *ca.* 1.17. This effect was significantly different for THF (the only non-multidentate solvent), where the α parameter remained largely unchanged at 0.62.

THF is known to bind to four sites on the lithium ion, and likely maintains coordinative saturation both when the ratio of lithium:oxygen is 0.025:1 and when it is 0.25:1; in both cases the relatively bulky THF surrounds the metal centre and the hydrogen bond donating ability is limited. This data does not conclusively indicate that the lithium is solvated by four THF molecules, since contact ion pairs are known and could have become significant at this concentration. However, the lithium ion is nevertheless ‘shielded’ from the Kamlet-Taft probe by the THF molecules.

The glyme molecules contain enough oxygen atoms to theoretically achieve similar coordinative saturation (four coordinated oxygen atoms per lithium cation) in the THF case. However, this effect only occurred at the dilute ratio of 0.025:1; the higher α value in the 0.25:1 ratio is strongly indicative of coordinatively unsaturated lithium cations being present. This effect is likely because at a ratio of 0.25:1, the lithium cation to glyme molecule ratio is extremely low (from 2 to 0.8 solvent molecules per lithium cation), indicating that the glyme molecules would have to adopt an entropically disfavoured state in order to fully enclose the lithium ion, coordinate to four binding sites, and achieve coordinative saturation. This situation clearly does not occur, and this observation is mirrored by neutron scattering data in the literature.²

The β parameter represents the hydrogen bond accepting ability of the solvent. The β parameters are relatively high in

ⁱⁱ It should be noted that these dilute solutions have a molality between 0.3 and 0.6 mol kg⁻¹.

the case of the pure solvents, due to the oxygen atoms not being coordinated and thus free to act as hydrogen bond acceptors. The values for all five molecular solvents are similar and for all four glymes are the same with error, due to the similar environments each oxygen atom is in (*i.e.* covalently bonded to two alkyl carbons).

In the dilute lithium solutions, the β parameter remains unchanged compared to the pure solvents. This result is because only a sub-stoichiometric amount of lithium has been added, relative to the number of oxygen centres. As such, the majority of the solvent molecules remain uncoordinated and are thus able to act as hydrogen bond acceptors.

Upon moving to the more concentrated ('solvate ionic liquid') systems, the β parameter drops significantly; this is consistent with more of the solvent being bound into the solvation spheres of the lithium. THF was the least affected, likely because the glymes are more influenced by adjacent oxygen atoms, *e.g.* coordination of one oxygen to lithium should influence the adjacent oxygen(s), both sterically and electrostatically.

The π^* parameter refers broadly to the dipolarity and polarisability of the system. Generally, the values for all five pure solvents were very similar, as was the case for α and β parameters. The absolute π^* values increased in the dilute lithium solutions compared to the pure glymes, from *ca.* 0.63 to *ca.* 0.72; THF was notable in having the smallest increase, while G3 demonstrated the largest increase. This same trend was also observed upon moving to the more concentrated lithium solution, where π^* increased to *ca.* 0.94; the THF case was significantly lower than all the glymes at 0.81. The increases in π^* upon addition of the lithium salt are consistent with addition of ions, where charge separation of ions enhances the solution's ability to support an electric field, increasing its polarisability, and with the charges contributing to the polarity of the solvent. The spherical symmetry of the lithium ion allows the ligands to rapidly convert between coordination geometries³⁶ allowing lithium complexes to distort to support an electrical field, once again likely increasing the polarisability of such media.

Notably, the Kamlet-Taft parameters for the THF cases were largely indistinguishable from those of the four glymes, both in their pure state and as a dilute lithium solution. For the concentrated lithium salt cases, THF was consistently different from the glymes in all three parameters; this dissimilarity is perhaps consistent with the monodentate THF maintaining similar degrees of solvation at lithium:oxygen ratios of both 0.025:1 and 0.25:1. Conversely, the glymes are not able to completely solvate the lithium ion to the same degree at a ratio of 0.25:1, leaving some regions of the lithium ion exposed and thus significantly affecting the Kamlet-Taft parameters. For the concentrated lithium solutions in glymes, the following trends were observed;

α	G3	<<<	G1	<	G2	<<	G4
β	G3	<	G4	<	G2	<<	G1
π^*	G1	<<	G2	<	G4	<	G3

These data express that (i) α in G3 increased by the least, (ii) β in G3 decreased by the most, and (iii) π^* in G3 increased by the most.

NMR spectroscopic analysis

The mixtures described above were each analysed using NMR spectroscopy. Particularly, the change in the chemical shift of key nuclei upon addition of Li[Tf₂N] was determined. For the THF containing systems, only the methylene groups adjacent to the oxygen were analysed. It is important to note that in each spectrum no distinction could be made between glymes in different complexation environments, indicating that there is a rapid exchange on the NMR time scale between free and coordinated glyme. For the lithium NMR cases, either there is only a single coordination environment or, more likely, there is a rapid equilibrium between coordination environments. NMR signals observed are tabulated in Table S2.

⁷Li NMR Spectroscopic analysis

The ⁷Li NMR data shows a significant difference in the chemical environment of the lithium ion between the various mixtures analysed (Figures 2 and S2). First of all, it is important to note that the signals are all moved to a lower chemical shift from the reference. In the dilute mixtures (0.025 lithium ions per oxygen), a trend was observed in the G1 through G4 cases, with an increase in the chemical shift with increasing size of the glyme. This trend indicates greatest shielding of the lithium in the G1 system and the least shielding in the G3 and G4 cases, with negligible difference between the latter two.

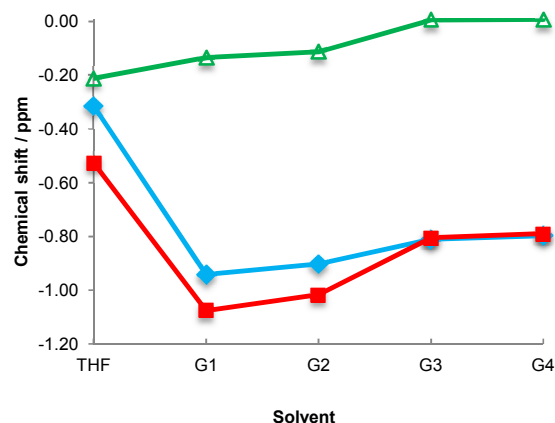


Figure 2. ⁷Li NMR chemical shifts for systems containing either THF, G1, G2, G3 or G4 with Li[Tf₂N] at a concentration corresponding to either 0.025 (blue diamonds, ♦) or 0.25 (red squares, ■) lithium ions per solvent oxygen referenced to 9.7 mol kg⁻¹ LiCl in H₂O, as well as the change upon moving from the former to the latter systems (green triangles, ▲).

This trend is likely the result of two effects; the donation of electrons to the lithium centre by the glyme ligands and the (more significant) donation of electrons by the Tf₂N⁻ counter-ion; notably the chemical shifts are close to those previously reported for ion pairing in similar systems.²⁶ It is the balance of these two effects, both of which should change the chemical shift of the signal in the same direction (as both

involve the donation of electron density to the lithium centre) that is important. The G1, which coordinates the lithium centre less effectively than the other glymes,³ has less donation of electron density by the glyme but is also less able to inhibit interaction of the lithium centre with the Tf_2N^- counter-ion.³ The greater interaction of the lithium with the counter-ion in this case (*cf.* other glyme cases), would result in more electron density being donated to the lithium ion and thus a more shielded system with a more negative chemical shift. The argument in each of the G3 and G4 cases are related to this one; with stronger coordination of the glyme to the lithium, the Tf_2N^- counter-ion is excluded to a greater degree, resulting in a more positive chemical shift. The larger glymes would also introduce steric issues, given the relatively large size of the Tf_2N^- anion.

The THF case does not fit the trend of the ^7Li chemical shifts observed in the presence of the glymes. This situation is likely due to the different steric bulk of the THF compared to the glymes, resulting in different coordination of the lithium ion with THF and the Tf_2N^- counter-ion. This difference makes a direct comparison between THF and the glyme cases particularly difficult. As such a concentration dependent study is more suitable for making comparisons.

The first thing to note when considering the concentrated systems (0.25 lithium ions per oxygen) is that the trend on changing the solvent is the same as for the dilute case, for the reasons presented above. On considering the change in the chemical shift between the dilute and concentrated cases (Figure 2, green triangles), the signals in the concentrated cases are observed with a lower chemical shift (*cf.* the dilute solutions) in the cases involving the small chain length glymes. This lower chemical shift is consistent with increased donation of electron density from the Tf_2N^- counter-ion, as supported by ion pairing studies.²⁶ The difference between the dilute and concentrated cases is primarily driven by an increase in the $\text{Li}[\text{Tf}_2\text{N}]$ concentration increasing the likelihood of interaction between the lithium ion and the Tf_2N^- counter-ion. The difference decreases upon moving to the larger glymes. As discussed above, as the glyme length increases it is better able to coordinate to the lithium centre and thus it is more able to exclude interaction with the counter-ion. As such, the importance of changing the concentration of the $\text{Li}[\text{Tf}_2\text{N}]$ in solution is not as marked in these cases. However this trend is not a simple linear correlation, with smaller changes in the chemical shift of the signal (relative to the dilute solutions) upon moving to a solution with an integer number of glyme molecules per lithium ion (G1 and G3, with a ratio of glyme to lithium of 2:1 and 1:1, respectively).

^{17}O NMR Spectroscopic analysis

For the ^{17}O NMR data (Figure S3), all signals shifted to a lower chemical shift relative to the pure solvents upon addition of $\text{Li}[\text{Tf}_2\text{N}]$. This shift mirrors what has been previously reported for similar systems, and was rationalised based upon electron withdrawal from the oxygen towards the lithium ion resulting in an electron poor oxygen atom.³⁷ While this effect contradicts the simple view of electron density shielding, this

effect has been specifically shown for aliphatic ethers where withdrawal of electron density results in a more shielded system and thus a lower chemical shift.³⁸

For the dilute cases, the signals due to the non-terminal oxygen centres (those not adjacent to a methyl group) show the same change in the chemical shift of the signals (relative to the corresponding signals in the pure glymes) in the presence of the lithium salt, irrespective of the ligand present (Figure S4). This similarity indicates similar interactions with the lithium ion in each case, which is reasonable because these oxygen atoms have similar electronic properties in the pure glymes and they have similar positions in the molecule.

The signals attributed to the terminal oxygen atoms (those adjacent to a methyl group) show a smaller change in chemical shift (relative to the corresponding pure glyme) upon addition of the $\text{Li}[\text{Tf}_2\text{N}]$ than the non-terminal oxygen atoms; this difference indicates a smaller effect of the lithium ion on the terminal oxygen atoms than on the non-terminal oxygen atoms. This smaller effect is likely due to a lower extent of coordination of the lithium by the oxygen centres at these terminal sites; the oxygen atoms spend less time (on average) bound to the lithium nucleus resulting in a shift of smaller magnitude.

Additionally, the change in chemical shift upon addition of the lithium salt for the terminal oxygen atoms varies with the glyme used. Upon moving from G1 to G2, a significant increase in the change in chemical shift (relative to the pure glyme) is observed. This change is likely due to the stronger binding in the G2 case (greater denticity). However, this trend does not continue to the G3 and G4 cases; this difference may appear to indicate that G2 binds more strongly to the lithium ion than G3 and G4, which is at odds with experimental results.³ The likely rationale is that coordination of lithium to the non-terminal oxygen atoms is favoured (on entropic grounds); G3 and G4 having more non-terminal oxygen centres decreases the extent of interaction of the lithium with the terminal oxygen atoms.

THF shows the same general effect as the glymes, with coordination to the lithium ion resulting in a lower chemical shift of the signal (relative to pure THF). However, the magnitude of the shift is not directly comparable to the glymes, due to the likelihood of significantly different binding environments.

For the concentrated lithium salt cases, only a single, very broad ^{17}O NMR signal was seen in the G2 through to G4 examples; accurately determining the chemical shift was not practical, which made any comparison impossible. However THF and G1 both showed a greater change in chemical shift (relative to the pure solvent) than in the dilute cases. This change in chemical shift is due to more lithium ions being present and thus a larger proportion of either the THF or glyme being coordinated to a lithium centre.ⁱⁱⁱ

ⁱⁱⁱ This is not a simple linear trend based upon concentration, with the change in chemical shifts being significantly less than that expected from such a correlation.

^1H NMR Spectroscopic analysis

The ^1H NMR data (Figure S5) showed a decrease in chemical shift of the signals of the glyme and THF upon addition of $\text{Li}[\text{Tf}_2\text{N}]$. This shift is consistent with what has been reported in the literature but which has not been rationalised.^{3, 27, 39} For the dilute glyme solutions, increasing the chain length of the glyme results in a decrease in the difference in chemical shift (dilute solution *cf.* pure glyme) of the signals (Figure 3), similar to the trend observed using lithium NMR spectroscopy. If this change was purely due to interactions with the lithium ions, the magnitude of the shift would be expected to be larger for the longer glymes due to the greater degree of coordination. These data suggest that interactions with the Tf_2N^- counter-ion are significant; such interactions are reduced for a more complexing multidentate ligand.

Additionally, it was observed that the ^1H NMR signals due to the methylene groups shifted less than those due to the methyl groups upon addition of the lithium salt (Figure 4). This difference again indicates interaction with the counter-ion is significant. If the interaction with lithium was the only significant interaction then the methylene protons would be affected by two oxygen atoms coordinating to the lithium *cf.* to the single oxygen atom for the methyl group, resulting in a greater effect on coordination in the former case; this was not observed.

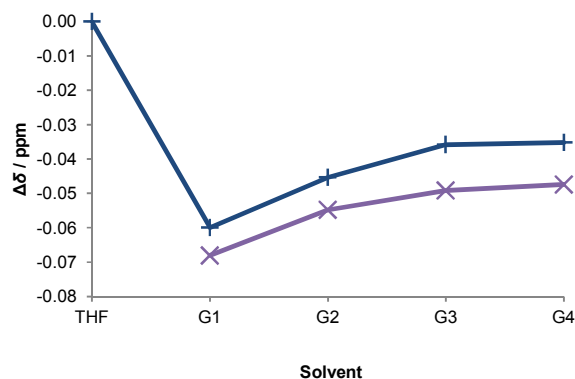


Figure 3. ^1H chemical shift of signals due to methyl (purple X), and representative methylene (blue +) groups in systems containing either THF, G1, G2, G3 or G4 with $\text{Li}[\text{Tf}_2\text{N}]$ in a concentration corresponding to 0.025 lithium ions per solvent oxygen, relative to the corresponding signals in the pure solvent. The methylene groups considered on the THF are those next to the oxygen.



Figure 4. Diagram showing a portion of the coordination environment of the lithium ion showing the methyl and methylene groups.

These trends can be understood by combining the effects of electron withdrawal by coordination to the lithium centre and electron donation by the Tf_2N^- counter-ion with a conventional understanding of electron density shielding the

nucleus, resulting in a lower chemical shift. Coordination of one of the oxygen donor ligands results in a reduction in electron density about the protons, which would result in a higher chemical shift. However this decreased electron density also makes them more likely to interact with the Tf_2N^- counter-ion, which would result in greater shielding and thus an overall lower chemical shift. The balance of these two effects results in the overall change in chemical shift being small.

The interaction with the lithium centre results in a greater effect (*i.e.* a greater extent of deshielding) on the methylene protons than on the methyl protons, due to the withdrawal of electrons by two oxygen atoms and thus two lithium-oxygen interactions for the methylene protons *cf.* a single oxygen for the methyl protons. This double effect results in the overall change in chemical shift of the signals (relative to the corresponding signals in the pure glymes) due to the combination of the interactions with the lithium and Tf_2N^- ions being less for the methylene protons than for the methyl protons. Similarly, as the chain length of the glyme is increased, the interaction with the lithium centre is increased, resulting in a reduced (relative to the shorter glymes) overall change in chemical shift (relative to the pure glyme).

THF is, once again, an outlier in the trends discussed. This feature is, once again, likely due to its significantly different structure compared to the other ligands. This structure inhibits interactions between the alpha protons and the Tf_2N^- counter-ion, reducing the shielding contribution and the overall change in chemical shift of the protons. Upon moving to the concentrated lithium salt case, all signals have a greater change in chemical shift, consistent with the results described above. However, like the oxygen NMR case, this is not a linear effect.

 ^{13}C NMR Spectroscopic analysis

For the ^{13}C NMR data, the signals due to the carbon atoms in the methyl group show no change (within uncertainty) in chemical shift upon addition of $\text{Li}[\text{Tf}_2\text{N}]$ (Figure S6). This absence of shift shows the balance between the effects of interaction of the ligand with the lithium ion and with the Tf_2N^- counter-ion, with these two effects likely cancelling one another to produce no observable change in chemical shift.

For the dilute lithium salt solutions the signals due to the methylene carbon atoms on the glymes show a small decrease in chemical shift upon addition of $\text{Li}[\text{Tf}_2\text{N}]$ (Figure S7). This decrease in chemical shift of the signals (relative to the corresponding signals in the pure glyme) is again a result of the combination of two effects; the interaction with the lithium ion withdrawing electron density and the interaction with the Tf_2N^- counter-ion donating electron density. Unlike the methylene protons, these methylene carbons are more affected by the Tf_2N^- interaction than the respective methyl cases, demonstrated by a greater decrease in chemical shift. This is likely a result of the carbons being able to withdraw electron density from multiple protons in the ethylene linkage, resulting in a more significant effect on the carbons and a less significant effect on the protons in the ethylene linkage. The

THF case shows no change in chemical shift (within uncertainty).

For the concentrated salt solutions, the signals due to the methylene carbons on the glymes showed a greater decrease in chemical shift than in the dilute cases, consistent with the results above and addition of more $\text{Li}[\text{Tf}_2\text{N}]$. As per the oxygen and proton NMR data, this decrease in chemical shift was not a linear relationship.

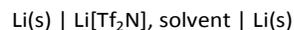
The THF case showed a small increase in chemical shift relative to the pure THF. This change from the glymes mirrors the proton NMR case where the Tf_2N^- counter-ion has either less interaction with or a reduced effect of interaction on the THF methylene group, which results in a reduced shielding component of the shift. However, unlike in the proton NMR spectroscopy case, the carbon NMR spectra of the concentrated cases show a higher chemical shift due to interactions with the lithium being dominant, resulting in an overall higher chemical shift relative to pure THF.

For the NMR analysis of the Tf_2N^- anion, due to the small changes in the chemical shift in the carbon NMR spectra (Figure S8) and the broad signals in the oxygen NMR spectra (Figure S3), there were no significant trends in the chemical shifts of the NMR active nuclei studied of the anion. Additionally, the large size of the anion will result in significant interaction with the components of the solutions other than lithium, even if it were coordinated to the lithium. As such, the chemical shifts of the glyme molecules are of greater interest.

These data show that the interactions between the lithium ion and the glyme ligands are not the only significant interactions in solution; rather, there are also significant interactions with the Tf_2N^- counter-ion. The longer the glyme chain length, the more significant the interactions between the glyme ligand and the lithium ion and the less significant the interaction between the lithium ion and Tf_2N^- counter-ion; the longer chain length glymes significantly impede these interactions, even in the concentrated case. Also a large portion of the interactions between the glyme ligand and lithium ion occurs at the non-terminal oxygen atoms, with the effect on the signals corresponding to these oxygen atoms being equal across the different chain length glymes. The effect of the interactions with the Tf_2N^- is dominant in the proton NMR cases and in the carbon NMR cases for methylene signals, with these interactions outweighing the effects of the lithium-glyme interactions. The THF cases were consistently found to be outliers, showing either the significant effect of polydentate solvents, or that this ether makes a poor substitute for extending the series of glymes to G0.

Thermoelectrochemical measurements

Thermoelectrochemical measurements were performed using the dilute and the concentrated solutions of lithium salt. They were placed between two lithium foil electrodes inside a hermetically-sealed casing, to measure the cell assembly represented below;



One electrode was heated and the other was maintained at a constant temperature, in order to measure the Seebeck coefficient (S_e), the temperature-dependence of the cell potential, in mV K^{-1} . The Seebeck coefficients for the various systems are shown in Figure 5.^{iv}

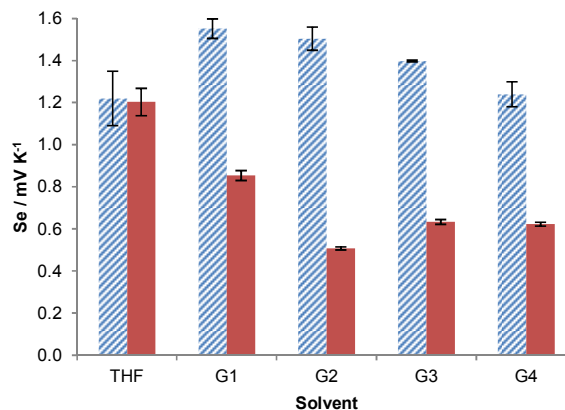


Figure 5. Seebeck coefficients of $\text{Li(s)} \mid \text{Li}[\text{Tf}_2\text{N}] \mid \text{Li(s)}$ for systems containing 0.025 lithium ions per oxygen atom (blue, diagonal lines) and 0.25 lithium ions per oxygen atom (red, solid fill).

In all cases, the Seebeck coefficients for these systems were positive. This sign indicates that oxidation was occurring at the cooler electrode, to form a more ordered state (lower entropy), and corresponds to electrodisolution of the bulk lithium metal to form a solvated lithium ion; this has been previously proven by observation of lithium migration in a G4-based cell.⁹ The solvated lithium ion is more ordered than the lithium metal, due to the significant effect from the introduction of the cation, effectively 'immobilising' the solvent in the solvation sphere. The hotter electrode correspondingly grows by electrodeposition, with the entropic driving force behind this entire process being release of the solvating ligand; therefore the Seebeck coefficient should be strongly correlated with the degree of interaction between the solvent and the lithium cation (and potentially the Tf_2N^- anion).

In the dilute electrolyte case (0.025 lithium ions per oxygen on the solvent), the Seebeck coefficients for all five solvents are *ca.* $1.4 \pm 0.2 \text{ mV K}^{-1}$; this is consistent with all of them being solutions of lithium cations solvated in ethereal solvents, hence similar results are observed (as for the Kamlet-Taft results). A notable minor trend was the Seebeck coefficient in the glyme systems decreasing as the chain length increases (G1, $1.55 \pm 0.05 \text{ mV K}^{-1}$; G4, $1.23 \pm 0.04 \text{ mV K}^{-1}$), consistent with more significant packing or solvation by the smaller glyme

^{iv} An example measurement (Figure S10) and the Seebeck coefficients for additional concentrations (Figure S11) are shown in the ESI.

molecules. All of the glymes demonstrated a higher Seebeck coefficient than THF, consistent with their higher density, and the fact that one oxygen coordinating to the lithium cation can impact the non-coordinating oxygen(s) on the same molecule.

In the concentrated “solvate ionic liquid” cases (which corresponds to 0.25 lithium ions per oxygen atom) the Seebeck coefficients of the systems no longer follow the simple trend observed in the dilute systems. Instead, the value for THF was essentially unchanged while values for all the glyme cases were significantly lower. The Seebeck coefficient in the G1 case remained the highest, that for the G2 case was the lowest, and the Seebeck coefficients for the G3 and G4 cases were both slightly higher than in the G2 case.

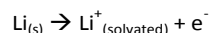
The Seebeck coefficient corresponds to a complete (de)solvation process, since it covers bulk lithium metal and the solvated lithium ion cation. As such, the degree of solvation for the redox-active lithium cation was quantitatively estimated for each of the solvent systems.

Calculation of lithium coordination from the Seebeck coefficient

The Seebeck coefficient (S_e) is a quantitative expression of the overall entropy change occurring in a redox process (ΔS), as shown by Equation 2; n is the number of electrons involved in the redox process and F is Faraday’s constant.

$$\Delta S = S_e n F \quad (2)$$

The measured Seebeck coefficients correspond to ΔS values in the range of *ca.* +60 to +190 J K⁻¹ mol⁻¹ (full details in ESI). These data can be related to the changes that must have occurred during the redox process to achieve this change in entropy, namely



The entropy of electron transfer/transport is known to be negligible, compared to the relatively large entropy changes for the overall process.⁴⁰ Hence, removing the electron from consideration, a consistent process in all systems was the entropy change associated with the loss of ordered lithium metal; Schmidt *et al.* have calculated this from the melting entropy of Li_(s) and volume changes upon solution formation to be *ca.* +42 J K⁻¹ mol⁻¹.⁴¹

All remaining entropic considerations relate to the solvent structuring around the Li⁺; the solvent will be immobilised in the primary solvation sphere, and partially immobilised in the secondary (Born) layer. The Born layer values were estimated based upon the hard sphere radius of the solvent and its dielectric constant; full details are shown in the ESI (values in Table S3), but decreased consistently from THF (*ca.* -65 J K⁻¹ mol⁻¹) to G4 (*ca.* -37 J K⁻¹ mol⁻¹).

Knowing the overall entropy change, the fixed entropic contribution estimated for ordered lithium metal formation/loss, and the minor contribution occurring in the Born layer, the remaining entropic contribution corresponds to the solvent in the inner solvation sphere. Here the solvent can be considered to be immobilised, and therefore the

entropy of fusion of the solvent allows prediction of how many molecules (or even what fraction of a longer molecule) was immobilised in the inner solvation sphere. The full calculations for this model are shown in the ESI (values in Table S4 and S5), but the estimated solvent oxygen atoms involved in the solvation of the lithium cation are shown graphically in Figure 6. This methodology is based upon treating each oxygen unit as a free segment, with that segment of the solvent immobilised upon coordination to the lithium cation.

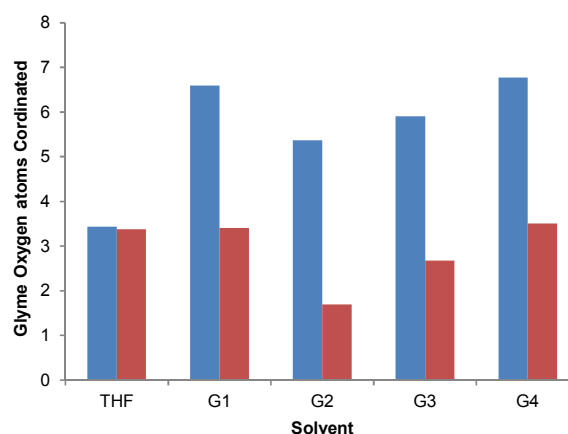


Figure 6. Calculated number of glyme oxygen atoms coordinated per lithium ion for the dilute lithium salt cases (blue) and concentrated lithium salt cases (red).

It must be emphasised that Figure 6 is based upon a series of approximations and assumptions. However, the calculated environment for THF is *ca.* 3.5 oxygen atoms (or [Li(THF)_{3.5}]⁺), in both the dilute and concentrated situations; THF has been shown to only bind to four sites on lithium,^{42, 43} hence this calculation matches well with reported values.

In contrast to the THF cases, the G1 dilute system predicted near complete solvation of the Li⁺ with *ca.* 6.6 oxygen groups (or up to 4 G1 molecules) involved. Four G1 molecules might be considered equivalent to two 12-crown-4 ether molecules, and the latter has been shown to achieve octahedral solvation of Li⁺ via all eight of their oxygen atoms, in the solid state.³⁶

In general, all estimated values were similar to, but slightly below values reported using other techniques. For example, crystal structures of 1:1 G3:Li⁺ have found all 4 oxygen atoms bound to Li⁺,⁴⁴ while the Seebeck coefficient for the 1:1 liquid system here corresponded to approximately 2.7 oxygen atoms. The crystal structure of 2:1 G2:Li[Tf₂N] has also been reported, with all 6 glyme oxygen atoms coordinated to the Li⁺,⁴⁴ the Seebeck coefficient measured in the dilute G3 system here also corresponded to 5.9 oxygen atoms. A recent combined neutron scattering and computational investigation of the solvation environment of a 1:1 mixture of Li[Tf₂N]:G3 reported a glyme oxygen solvation number of 3.4;⁴⁵ the Seebeck coefficient measured here corresponds to *ca.* 2.7 oxygen atoms.

Notably, these approximations exclude the role of Tf_2N^- in solvation, yet the role of the oxygen atoms in this anion in solvating Li^+ (as contact ion pairs) has been demonstrated in both crystal structures⁴⁴ and neutron scattering experiments on solvate ionic liquids.⁴⁵ The immobilisation of an entire Tf_2N^- anion in solvating a Li^+ is predicted to be the entropic equivalent of 0.8 THF molecules, or 0.08 G4 molecules (or 0.4 G4 oxygen atoms). This contribution is due to the considerably greater flexibility of the latter relative to the former, and the relatively limited entropic contribution predicted for the immobilisation of a Tf_2N^- anion (ca. $-28 \text{ J K}^{-1} \text{ mol}^{-1}$).⁴⁶ However, contact ion pair formation would presumably reduce the Born contribution (due to charge screening) and thus glyme oxygen solvation numbers would increase, corresponding closely with literature values. Ultimately, more information is required to identify the extent of ion pair formation, and the nature of charge screening (especially in the most concentrated media) before such predictions can be made truly quantitative. Nevertheless, these preliminary predictions match both the solid-state and liquid-state literature trends well; this indicates that further work in this area is strongly merited.

Comparisons between Kamlet-Taft solvent parameters, NMR chemical shifts and thermoelectrochemical measurements

The three methodologies utilised in this study involve fundamentally different interactions. The Kamlet-Taft solvent parameters are based upon how the solution interacts with solvchromatic dyes, specifically through hydrogen bonding and non-specific electronic interactions. NMR spectroscopy evaluates the electronic interactions that result in (de)shielding of the nucleus being analysed. The Seebeck coefficient is a measure of the entropy change upon electro-dissolution/electrodeposition of the lithium metal, which is highly dependent upon the interactions of the lithium ion with the solvating molecules in solution.

As these three methodologies involve fundamentally different interactions, and there is significant clustering of data in some cases, direct quantitative correlations are challenging and of limited practicality. However, some qualitative comparisons can be made.

THF was consistently observed to be an outlier, acting quite differently to the other glymes. The Kamlet-Taft parameters showed significantly less change upon addition of $\text{Li}[\text{Tf}_2\text{N}]$ as compared to the glymes, the NMR chemical shifts for the THF cases did not fit the trends for G1-G4 cases, and the Seebeck coefficient showed no change between the concentrated and dilute solutions for this solvent.

Comparing the Kamlet-Taft parameters to the NMR analysis is complicated due to the multitude of signals which could be compared and multiple contributing effects to any changes observed. What can be seen is that the NMR signals typically follow simple trends as the glyme chain length is varied; this is not seen in the Kamlet-Taft parameters. However a similarity between the NMR and Kamlet-Taft data is the change upon addition of lithium; in general there is an effect on the NMR chemical shift and the Kamlet-Taft parameters when comparing the pure solvent and dilute

solution cases and this effect is increased in magnitude in the concentrated cases.

In comparing the NMR data to the Seebeck coefficients, the most meaningful comparison is that involving the lithium NMR spectroscopy, as the coordination of the lithium has the potential to effect both the NMR chemical shift and the Seebeck coefficient. In the dilute salt cases a similar trend is observed for both ^7Li chemical shifts and the Seebeck coefficient. The ^7Li chemical shift is the lowest (*i.e.* the most shielded) for lithium in G1, with the chemical shift increasing as the glyme chain length is increased up to G4, and lithium in THF has the largest chemical shift. This effect is mirrored by the Seebeck coefficient, which is highest for lithium in G1, decreasing as the chain length of the glyme increases to G4, with THF the same within error as G4. However, this similarity is not present for the concentrated salt cases.

Finally, when comparing Kamlet-Taft parameters to the Seebeck coefficient, the parameters most likely to contribute are the β and π^* parameters; the β parameter, indicating hydrogen bond accepting ability, can indicate how well solvent molecules can coordinate to the lithium ion, while the π^* parameter indicates the solvent polarities, which can indicate how well the solvent molecules can organise around the lithium ion. It was observed that in general a high β and a low π^* parameter correlated with a large Seebeck coefficient; however this was primarily from two clusters of data (see Figure S12 and Table S6 in the ESI).

Conclusions

This work has probed the properties of several $\text{Li}[\text{Tf}_2\text{N}]^-$ and glyme-based solvate ionic liquids, their dilute solutions and their parent solvents, using a range of methods. The Kamlet-Taft solvent parameters were quantified; the dilute solutions demonstrated similar values and limited trends. The solvate ionic liquids displayed significantly different values, and greater dissimilarity between the various systems. Importantly, it also demonstrated incomplete solvation of the lithium ion by the glymes, and that the solvate does not always interact as a large, charge diffuse cation.

Detailed NMR analysis using ^1H , ^7Li , ^{13}C and ^{17}O was also performed. NMR chemical shifts indicated a significant interaction between the lithium ion and the Tf_2N^- counter-ion, with larger chain length glymes being more capable of excluding these interactions. This also further supported incomplete coordination of the lithium cations.

Thermoelectrochemical measurements of these systems in contact with lithium metal demonstrated that the dilute lithium-glyme based electrolytes, as well as lithium-THF based electrolytes, have large Seebeck coefficients (up to 1.6 mV K^{-1}). This significant temperature-sensitivity can be applied for thermoelectrochemical applications, but can also detrimentally influence devices such as batteries. The more concentrated (solvate ionic liquid-based) systems demonstrated significantly lower values, once again indicative of the lack of coordinative saturation of the lithium by the glymes.

The determined Seebeck coefficients allowed approximation of the number of solvent oxygen atoms coordinated to the lithium ion. These values matched literature trends well, but were consistently lower; this is consistent with the ion pair formation highlighted by the NMR studies.

In this work, Kamlet Taft parameters have been shown to have a qualitative correlation to Seebeck coefficients of lithium in lithium glyme based electrolytes, with the α and π^* parameter showing a small negative correlation and the β parameter showing a positive correlation. Further development of all three techniques in parallel will likely generate powerful predictive tools for a range of applications, but a wider range of Li[TF₂N]-glyme ratios and different glyme structures need to be investigated. In all cases THF was an outlier, indicating it isn't a suitable substitute for dimethyl ether to continue the series of glymes.

Conflicts of Interest

There are no conflicts of interest to declare.

Acknowledgements

This work was supported by an Australian Government Research Training Program Ph.D. Scholarship and an Australian Research Council grant (DE130100770). The authors would like to thank the NMR facility of the Mark Wainwright Analytical Centre at UNSW for NMR support. ARC grant LE120100027 contributed towards purchase of NMR equipment.

References

1. K. Ueno, K. Yoshida, M. Tsuchiya, N. Tachikawa, K. Dokko and M. Watanabe, *J. Phys. Chem. B*, 2012, **116**, 11323-11331.
2. T. Murphy, S. K. Callear, N. Yepuri, K. Shimizu, M. Watanabe, J. N. Canongia Lopes, T. Darwish, G. G. Warr and R. Atkin, *Phys. Chem. Chem. Phys.*, 2016, **18**, 17224-17236.
3. C. Zhang, K. Ueno, A. Yamazaki, K. Yoshida, H. Moon, T. Mandai, Y. Umebayashi, K. Dokko and M. Watanabe, *J. Phys. Chem. B*, 2014, **118**, 5144-5153.
4. L. Carbone, M. Gobet, J. Peng, M. Devany, B. Scrosati, S. Greenbaum and J. Hassoun, *ACS Appl. Mater. Interfaces*, 2015, **7**, 13859-13865.
5. K. Ueno, J.-W. Park, A. Yamazaki, T. Mandai, N. Tachikawa, K. Dokko and M. Watanabe, *J. Phys. Chem. C*, 2013, **117**, 20509-20516.
6. K. Yoshida, M. Tsuchiya, N. Tachikawa, K. Dokko and M. Watanabe, *J. Electrochem. Soc.*, 2012, **159**, A1005-A1012.
7. T. Tamura, K. Yoshida, T. Hachida, M. Tsuchiya, M. Nakamura, Y. Kazue, N. Tachikawa, K. Dokko and M. Watanabe, *Chem. Lett.*, 2010, **39**, 753-755.
8. H.-M. Kwon, M. L. Thomas, R. Tatara, Y. Oda, Y. Kobayashi, A. Nakanishi, K. Ueno, K. Dokko and M. Watanabe, *ACS Appl. Mater. Interfaces*, 2017, **9**, 6014-6021.
9. J. J. Black, T. Murphy, R. Atkin, A. Dolan and L. Aldous, *Phys. Chem. Chem. Phys.*, 2016, **18**, 20768-20777.
10. D. J. Eyckens, M. E. Champion, B. L. Fox, P. Yoganantharajah, Y. Gibert, T. Welton and L. C. Henderson, *Eur. J. Org. Chem.*, 2016, **2016**, 913-917.
11. K. Ueno, J. Murai, K. Ikeda, S. Tsuzuki, M. Tsuchiya, R. Tatara, T. Mandai, Y. Umebayashi, K. Dokko and M. Watanabe, *J. Phys. Chem. C*, 2016, **120**, 15792-15802.
12. K. Yoshida, M. Tsuchiya, N. Tachikawa, K. Dokko and M. Watanabe, *J. Phys. Chem. C*, 2011, **115**, 18384-18394.
13. R. W. Taft and M. J. Kamlet, *J. Am. Chem. Soc.*, 1976, **98**, 2886-2894.
14. M. J. Kamlet and R. W. Taft, *J. Am. Chem. Soc.*, 1976, **98**, 377-383.
15. M. J. Kamlet, J. L. Abboud and R. W. Taft, *J. Am. Chem. Soc.*, 1977, **99**, 6027-6038.
16. J. Barbosa, G. Fonrodona, I. Marqués, S. Butí and I. Toro, *TRAC, Trends Anal. Chem.*, 1997, **16**, 104-111.
17. S. Şanlı, Y. Altun and G. Alsancak, *J. Solution Chem.*, 2012, **41**, 1352-1363.
18. R. W. Taft, N. J. Pienta, M. J. Kamlet and E. M. Arnett, *J. Org. Chem.*, 1981, **46**, 661-667.
19. C. Bizzarri, V. Conte, B. Floris and P. Galloni, *J. Phys. Org. Chem.*, 2011, **24**, 327-334.
20. B. R. Mellein, S. N. V. K. Aki, R. L. Ladewski and J. F. Brennecke, *J. Phys. Chem. B*, 2007, **111**, 131-138.
21. M. Holzweber, R. Lungwitz, D. Doerfler, S. Spange, M. Koel, H. Hutter and W. Linert, *Chem. Eur. J.*, 2013, **19**, 288-293.
22. R. Klein, O. Zech, E. Maurer, M. Kellermeier and W. Kunz, *J. Phys. Chem. B*, 2011, **115**, 8961-8969.
23. A. Dolan, D. A. Sherman, R. Atkin and G. G. Warr, *ChemPhysChem*, 2016, **17**, 3096-3101.
24. D. J. Eyckens, B. Demir, T. R. Walsh, T. Welton and L. C. Henderson, *Phys. Chem. Chem. Phys.*, 2016, **18**, 13153-13157.
25. A. Plewa, M. Kalita and M. Siekierski, *Electrochim. Acta*, 2007, **53**, 1527-1534.
26. A. Plewa-Marczewska, M. Kalita, M. Marczewski and M. Siekierski, *Electrochim. Acta*, 2010, **55**, 1389-1395.
27. K. Yoshida, M. Nakamura, Y. Kazue, N. Tachikawa, S. Tsuzuki, S. Seki, K. Dokko and M. Watanabe, *J. Am. Chem. Soc.*, 2011, **133**, 13121-13129.
28. T. I. Quickenden, *J. Electrochem. Soc.*, 1995, **142**, 3985-3994.
29. M. F. Dupont, D. R. MacFarlane and J. M. Pringle, *Chem. Commun.*, 2017, **53**, 6288-6302.
30. N. Cusack and P. Kendall, *Proc. Phys. Soc.*, 1958, **72**, 898-901.
31. J. J. Black, J. B. Harper and L. Aldous, *Electrochem. Commun.*, 2018, **86**, 153-156.
32. G. H. Lane, A. S. Best, D. R. MacFarlane, A. F. Hollenkamp and M. Forsyth, *J. Electrochem. Soc.*, 2010, **157**, A876-A884.
33. M. Al Maimani, J. J. Black and L. Aldous, *Electrochem. Commun.*, 2016, **72**, 181-185.
34. L. Aldous, J. J. Black, M. C. Elias, B. Gelinas and D. Rochefort, *Phys. Chem. Chem. Phys.*, 2017, **19**, 24255-24263.
35. R. Tatara, N. Tachikawa, H.-M. Kwon, K. Ueno, K. Dokko and M. Watanabe, *Chem. Lett.*, 2013, **42**, 1053-1055.
36. U. Olsher, R. M. Izatt, J. S. Bradshaw and N. K. Dalley, *Chem. Rev.*, 1991, **91**, 137-164.
37. J. Peng, L. Carbone, M. Gobet, J. Hassoun, M. Devany and S. Greenbaum, *Electrochim. Acta*, 2016, **213**, 606-612.
38. M.-T. Béraldin, E. Vauthier and S. Fliszár, *Can. J. Chem.*, 1982, **60**, 106-110.
39. S. Sun, Y. Niu, Q. Xu, Z. Sun and X. Wei, *RSC Adv.*, 2015, **5**, 46564-46567.

40. J. N. Agar, *Advances in Electrochemistry and Electrochemical Engineering, Vol 3*, Interscience Publishers, London, 1963.
41. M. J. Schmid, K. R. Bickel, P. Novák and R. Schuster, *Angew. Chem. Int. Ed.*, 2013, **52**, 13233-13237.
42. S. A. Cotton, F. A. Hart, M. B. Hursthouse and A. J. Welch, *J. Chem. Soc., Chem. Commun.*, 1972, **0**, 1225-1226.
43. J. L. Atwood, W. E. Hunter, R. D. Rogers, J. Holton, J. McMeeking, R. Pearce and M. F. Lappert, *J. Chem. Soc., Chem. Commun.*, 1978, **0**, 140-142.
44. W. A. Henderson, F. McKenna, M. A. Khan, N. R. Brooks, V. G. Young and R. Frech, *Chem. Mater.*, 2005, **17**, 2284-2289.
45. K. Shimizu, A. A. Freitas, R. Atkin, G. G. Warr, P. A. FitzGerald, H. Doi, S. Saito, K. Ueno, Y. Umebayashi, M. Watanabe and J. N. Canongia Lopes, *Phys. Chem. Chem. Phys.*, 2015, **17**, 22321-22335.
46. D. P. Fagnant, M. A. Desilva and J. F. Brennecke, *J. Chem. Eng. Data*, 2016, **61**, 958-967.